ACS EARTH AND SPACE CHEMISTRY

Article

Cite This: ACS Earth Space Chem. 2017, 1, 664–672

Criegee Intermediate–Alcohol Reactions, A Potential Source of Functionalized Hydroperoxides in the Atmosphere

Max R. McGillen,*[†] Basile F.E. Curchod,[†] Rabi Chhantyal-Pun,[†] Joseph M. Beames,[‡] Nathan Watson,[‡] M. Anwar H. Khan,[†] Laura McMahon,[†] Dudley E. Shallcross,[†] and Andrew J. Orr-Ewing*[†]

[†]School of Chemistry, University of Bristol, Cantock's Close, Bristol, BS8 1TS, United Kingdom

[‡]School of Chemistry, Cardiff University, Cardiff, CF10 3AT, United Kingdom

Supporting Information

ABSTRACT: Ozonolysis, the mechanism by which alkenes are oxidized by ozone in the atmosphere, produces a diverse family of oxidants known as Criegee intermediates (CIs). Using a combination of newly acquired laboratory data and global atmospheric chemistry and transport modeling, we find that the reaction of CIs with alcohols, a reaction that was originally employed to trap these reactive species and provide evidence for the ozonolysis mechanism nearly 70 years ago, is occurring in Earth's atmosphere and may represent a sizable source of functionalized hydroperoxides therein. Rate coefficients are reported for the reactions of CH_2OO and $(CH_3)_2COO$ with methanol and that of CH_2OO with ethanol. Substitution about the Criegee intermediate is found to have a strong influence over the reaction rate, whereas substitution on the alcohol moiety does not. Although these reactions are not especially rapid, both the precursors to CIs and alcohols have large emissions from the terrestrial biosphere, leading to a high degree of co-location for this chemistry. We estimate that the products of these reactions, the α-alkoxyalkyl hydroperoxides (AAAHs) have a production rate of ∼30 Gg year^{-1}. To assess the atmospheric lifetime of AAAHs, we used the nuclear ensemble method to construct a UV absorption spectrum from the four lowest energy conformers identified for a representative AAAH, methoxymethyl hydroperoxide. The computed absorption cross-section indicates that these compounds will be lost by solar photolysis, although not so rapidly as to exclude competition from other sinks such as oxidation, thermal decay, and aerosol uptake.

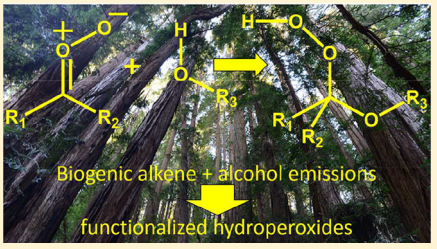

KEYWORDS: *Criegee, alcohol, kinetics, atmospheric chemistry, non-Arrhenius, hydroperoxide*

1. INTRODUCTION

Criegee intermediates (CIs), also known as carbonyl oxides, are a family of oxidants produced in Earth's atmosphere through alkene ozonolysis. The identity of a CI is determined by the alkene reagent, and as a consequence of its zwitterionic character, may exist in several forms with significant barriers to rotation between conformers.[1] In the ozonolysis of isoprene, for example, nine possible Criegee intermediates are produced.[2] The corollary of this is that the variety of CIs encountered in the atmosphere may exceed that of alkenes. Ozonolysis forms CIs that possess a range of internal energies, a varying proportion of which possess sufficient excitation for prompt decomposition. The remainder may be either collisionally stabilized or formed in a stabilized state. These stabilized CIs will be sufficiently long-lived with respect to unimolecular processes that they may also engage in bimolecular reactions.

Laboratory studies have identified a large diversity in the bimolecular reactivity among CIs. In the case of water dimer, $(H_2O)_2$, a rapid reaction (k_{298} = 7.4 × 10^{-12} cm^3 molecule^{-1} s^{-1}) is observed with formaldehyde oxide, CH_2OO,[3] yet no significant reactivity (k_{298} = < 1.5 × 10^{-16} cm^3 molecule^{-1} s^{-1}) is observed for acetone oxide, $(CH_3)_2COO$.[4] Conversely, both CIs react rapidly with SO_2, with $(CH_3)_2COO$ exhibiting a faster reaction rate.[4,5] It is therefore apparent that the reactivity of a given CI depends strongly upon both its structure and the identity of its reaction partner.

Despite having a low tropospheric concentration, estimated to be 5 × 10$^{4\pm1}$ molecule cm^{-3},[6] CIs have been identified as important oxidants of both SO_2[7,8] and organic acids.[9,10] Furthermore, among atmospheric oxidants, CIs are unusual in their capacity to add both carbon and oxygen mass to the co-reactant through 1,3-dipolar cycloaddition[11,12] and insertion mechanisms[13,14] and therefore have the potential to produce low-volatility products in comparatively few reaction steps, which may facilitate secondary organic aerosol (SOA) formation.

Alcohols are a prevalent class of volatile organic compounds in the atmosphere and have terrestrial biogenic sources,[15,16] of which tropical rainforests are among the largest. Because the highest flux of CIs is predicted to occur in the equatorial regions,[9,17] co-location is expected between CIs and alcohols in the troposphere, and the reactions between these species therefore warrant investigation. Such reactions are well-known

Received: September 21, 2017
Revised: November 8, 2017
Accepted: November 14, 2017
Published: November 14, 2017

DOI: 10.1021/acsearthspacechem.7b00108
ACS Earth Space Chem. 2017, 1, 664–672

to synthetic chemists and have found utility in the preparation of α-alkoxyalkyl hydroperoxides (AAAHs).[18] Similarly, in the gas phase, AAAHs have been identified in the reaction of CIs (CH_2OO, *syn*- and *anti*-tridecanal oxide) with alcohols (methanol, 2-propanol), all of which were studied using a static reaction chamber.[19,20] Tobias and Ziemann[20] reported a relative rate coefficient for these reactions, in which heptanoic acid was used as a reference compound. However, few direct kinetic data are available and to address this knowledge gap, a systematic study of the following reactions is conducted:

$$CH_2OO + CH_3OH \rightarrow \text{products} \quad (1)$$

$$CH_2OO + C_2H_5OH \rightarrow \text{products} \quad (2)$$

$$(CH_3)_2COO + CH_3OH \rightarrow \text{products} \quad (3)$$

Reaction 1 is an insertion reaction and the product has been identified as methoxymethyl hydroperoxide (MMHP).[19] A calculated UV absorption spectrum of MMHP is presented that allows its atmospheric photolysis lifetime to be assessed. This spectrum is found to closely resemble the experimentally measured spectra of analogous hydroperoxide species, and given the apparently generic similarity between these hydroperoxides, MMHP is used to represent the panoply of AAAHs that are expected to form from the reactions of larger, naturally occurring CIs with methanol. The atmospheric implications of these reactions are investigated through global chemistry transport modeling.

2. METHODS

2.1. Experimental Measurements. Rate coefficients for reactions 1−3 were determined at temperatures from 254−329 K and total pressures from 10−100 Torr using cavity ring-down spectroscopy (CRDS) to obtain temporal decay profiles of a flowing mixture of CH_2OO or $(CH_3)_2COO$ in the presence of a known excess of either methanol or ethanol. All rate coefficients were measured under pseudo-first-order conditions, where [alcohol] ≫ [CI]. The temperature of the reactor was controlled by circulating a heated or cooled fluid through an outer jacket, with a second insulating jacket employed to reduce temperature gradients across the reaction volume. A brief description of the apparatus and experimental technique is given below, with a fuller account provided by Chhantyal-Pun et al.[5,10]

Criegee intermediates, CH_2OO and $(CH_3)_2COO$ were generated through the photolysis (λ = 355 nm) of alkyl *gem*-diiodide precursors in the presence of excess O_2 according to the methodology of Welz et al.:[21]

$$CR_2I_2 + h\nu \rightarrow CR_2I + I \quad (4)$$

$$CR_2I + O_2 \rightarrow CR_2OO + I \quad (5)$$

where R = H or CH_3.

Signals of CH_2OO or $(CH_3)_2COO$ were probed using CRDS, the optical cavity of which was positioned at an angle of 3.8° with respect to the photolysis beam, providing a 7.6 cm long interaction region. The probe beam wavelength of 355 nm overlapped the broad and intense $\tilde{B}^1A' \leftarrow \tilde{X}^1A'$ electronic absorption bands of these CIs. Temporal decay profiles of CIs were generated by varying the delay time (i.e., reaction time) between the photolysis and probe beams. Under our experimental conditions, typical ring-down times (<6 μs) were much shorter than the time scales over which kinetic measurements were performed (1−14 ms).

These profiles were fitted with a simultaneous first- and second-order decay fit function shown in eq 6:[5]

$$\Delta\kappa(t) = \frac{k_p}{\frac{k_p}{\Delta\kappa(t_0)}e^{k_p t} - k'\left(\frac{2L}{cd}\right) + k'\left(\frac{2L}{cd}\right)e^{k_p t}} \quad (6)$$

where $\Delta\kappa(t)$ is the change in ring-down decay rate constant at delay time t caused by the photolysis laser, L is the cavity length (100 cm), d is the photolysis-probe laser overlap length (7.6 cm), c is the speed of light, k_p is the pseudo-first-order rate coefficient with respect to the alcohol reagent, and $k' = k_{obs}/\sigma_{355\ nm}$ is the second-order decay rate coefficient for the self-reaction of the CI scaled by its absorption cross-section at 355 nm. Because k' is temperature-dependent, a series of decay profiles were measured in the absence of alcohol over a range of temperatures, and these data were used to define a temperature-dependent function of the self-reaction, $k'(T)$, for use in this equation.

Alcohols were introduced into the reaction volume from a dilute bulb using a calibrated flow controller (MKS) over a range of concentrations, typically spanning a factor of ≥20. Concentrations were determined from the ideal gas law using the known mass flow rates from manometrically prepared bulbs, reactor temperature, and pressure. Bimolecular rate coefficients for reactions 1−3 were obtained from the slope of an error-weighted linear least-squares fit of k_p versus [alcohol]. In experiments with CH_3OD and CD_3OD because they possess the labile O−D moiety, D_2O was bubbled through the gas lines, mass flow controller, and reactor for 24 h prior to data acquisition.

2.2. Materials. Methanol (≥99.9%), ethanol (≥99.5%), CD_3OD (≥99.8 atom % D), CD_3OH (99.8 atom % D), CH_3OD (99.5 atom % D), diiodomethane (99%) (Sigma-Aldrich), and 2,2-diiodopropane (a high-purity sample was synthesized at the University of Edinburgh; see the Supporting Information for proton and carbon NMR spectra) were subjected to several freeze−pump−thaw cycles prior to their introduction into darkened 10 L Pyrex bulbs. D_2O (99.9 atom % D) (Sigma-Aldrich) was degassed but otherwise used as supplied. High-purity compressed gases N_2 (diluent and bath gas) and O_2 (reagent in reaction 5) (Air Liquide) were used as supplied.

2.3. Computational Calculations. For energy calculations, stationary points on the reaction pathways were optimized using DFT//B3LYP/aug-cc-pVTZ, all of which were verified through vibrational frequency calculations, and all transition states were linked to their respective minima through intrinsic reaction coordinate calculations. All geometries were generated using the Gaussian09 package.[22] Single-point energy calculations were performed at each stationary point using DF-HF//DF-LCCSD(T)-F12a/aug-cc-pVTZ. Both density fitting integral approximations and local correlation methods offer significant advantages in reducing computational cost when scaling to larger molecular systems and were used here to provide high-accuracy molecular energies. These calculations also include explicit electron correlation through use of the F12 ansatz, where F12a was chosen as the most appropriate treatment for this basis set. All energy calculations were performed using MOLPRO.[23] Recent calculations suggest that the CI moiety transitions from predominantly zwitterionic to biradical character during the course of a bimolecular

DOI: 10.1021/acsearthspacechem.7b00108
ACS Earth Space Chem. 2017, 1, 664−672

reaction,[24] which represents a major challenge for most computational electronic structure techniques. Multireference computational methods could be used in future for more detailed reaction pathway characterization.

For the calculation of absorption cross-sections, geometry optimizations of MMHP were conducted at the MP2 level of theory[25−28] using an aug-cc-pVTZ basis set[29] with Gaussian09[22] for four conformers (see the Supporting Information for details about the conformers and the level of theory employed). Frequency calculations confirmed that all localized extrema are actual minima of the ground-state potential-energy surface. A photoabsorption cross-section was then constructed for each conformer using the semiclassical[30−32] nuclear ensemble method as implemented in Newton-X version 1.4.[33,34] The nuclear ensemble technique samples a set of N_n nuclear geometries (200 in this case) from an approximate quantum distribution in the ground-electronic state. Excitation energies (E_{0n}) and oscillator strengths (f_{0n}) are then computed for each sampled geometry $\boldsymbol{R}_l$, and a photoabsorption cross-section $\sigma(E)$ is constructed by summing all the contributions using the equation:

$$\sigma(E) = \frac{\pi e^2 \gamma}{2mc\varepsilon_0} \sum_{n}^{N_s} \frac{1}{N_n} \sum_{l}^{N_n} f_{0n}(\mathbf{R}_l) g(E - E_{0n}(\mathbf{R}_l), \delta) \quad (7)$$

N_S is the total number of excited electronic states considered (1 in the present case) and $g(E - E_{0n}(\boldsymbol{R}_l),\delta)$ corresponds to a Lorentzian function with a width δ = 0.05 eV. The nuclear ensemble technique provides band shapes and heights, but it is important to note that it does not reproduce vibronic progressions.

The excitation energies and oscillator strengths for the transition to the first electronic state (S_1) were computed for all sampled geometries with the spin-component scaling second-order approximate coupled cluster (SCS-CC2) method,[35−37] using an aug-cc-pVDZ basis set,with the program Turbomole v6.4.[38] This level of theory was benchmarked against equation-of-motion coupled cluster singles and doubles (EOM-CCSD),[39] and a detailed comparison is presented in the Supporting Information.

2.4. Atmospheric Chemistry and Transport Modeling.

The atmospheric sources of AAAHs were quantified by incorporating the kinetic measurements of this study into the STOCHEM-CRI global atmospheric chemistry and transport model.[40] In the model, CIs are generated from six representative alkenes (ethene, propene, (*Z*)-2-butene, isoprene, α-pinene, and β-pinene). Because many more alkenes are emitted to the atmosphere than are present in the model, this limited selection is weighted to reflect the alkene functionality of the total biogenic alkene flux into the atmosphere,[41] which allows a realistic distribution of CIs at a reduced computational cost. Both the model and the methodology for generating CI fields have been used previously.[9,42] However, based on the availability of new experimental measurements and quantum calculations, these CI fields have been updated.[10] A full account of the stabilized CI yield from ozonolysis, the branching ratio between CIs, the unimolecular loss rate and rate coefficients for reactions with H_2O, $(H_2O)_2$, and methanol for each of the CIs contained within the model is provided in Table S4. By considering the production through the reactions of CIs with alcohols and the losses by photolysis and reaction with OH (by analogy to other hydroperoxides), the concentration of AAAH can be estimated in the model.

3. EXPERIMENTAL RESULTS

Experiments were conducted to measure the rates of reaction of CIs with methanol and ethanol. All kinetic data were fitted using a combined first- and second-order expression, eq 6 (see section 2.1) and temporal profiles of CIs were well described by these fits in all cases (Figure 1 shows a representative data set).

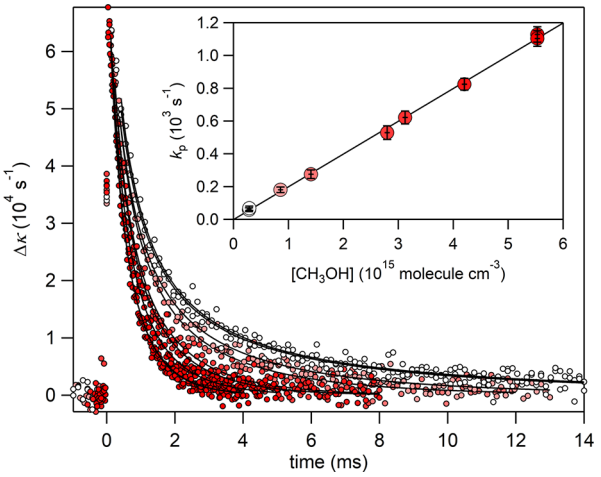

Figure 1. Series of kinetic decay traces acquired at 254 K showing progressively faster decays of CH_2OO as methanol concentration is increased. Solid lines are fits according to eq 6, from which the pseudo-first-order rate coefficients, k_p, are obtained. These values are plotted as a function of $[CH_3OH]$ in the inset, the slope of which yields the bimolecular rate coefficient. Error bars in the inset represent the 2σ statistical uncertainty of the fits.

In the experiments in which $(CH_3)_2COO$ was a reagent, a more rapid unimolecular decay occurred (~300 s^{-1}),[43] which manifested itself as an intercept in plots of k_p versus [methanol]. Rate coefficients were observed to be pressure-independent from 10−100 Torr (N_2). Rate coefficient data are plotted as a function of temperature in Figures 2 and 3 and

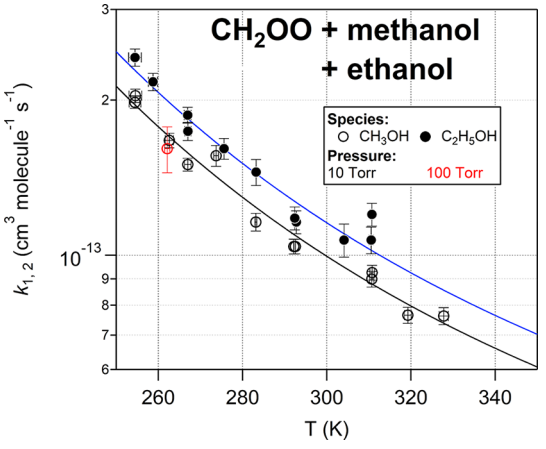

Figure 2. Bimolecular rate coefficients for the reactions of methanol and ethanol with CH_2OO exhibit a similar negative temperature dependence. Solid lines represent modified Arrhenius fits to data (see eqs 8 and 9). Error bars represent 2σ statistical uncertainty for rate coefficients and 1σ for temperature.

DOI: 10.1021/acsearthspacechem.7b00108
ACS Earth Space Chem. 2017, 1, 664−672

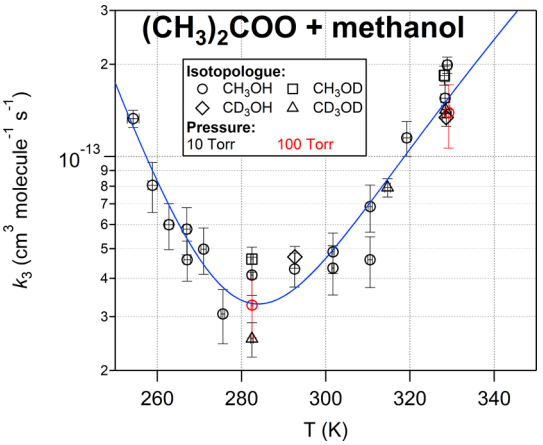

Figure 3. Bimolecular rate coefficient for the reaction of methanol with $(CH_3)_2COO$ exhibits both positive and negative temperature-dependent regimes. The solid line represents a sum of two expressions (see eq 10). Error bars represent 2σ statistical uncertainty for rate coefficients and 1σ for temperature.

show that reactions 1−3 each exhibit a negative temperature dependence, together with curvature, which is quite pronounced in the case of reaction 3. Kinetic data obtained in this study are presented in Tables S1−3, together with the experimental conditions that were employed; errors in rate coefficients are expressed as 2σ statistical uncertainty, and other errors are provided at 1σ.

3.1. Reactions of CH_2OO with CH_3OH and C_2H_5OH. Reaction 1, $CH_2OO + CH_3OH$, is the simplest of the reactions studied, with both reactants possessing one carbon atom. This reaction is expected to proceed through an insertion mechanism which produces CH_3OCH_2OOH (MMHP).[19]

Figure 2 shows the bimolecular rate coefficient, k_1, plotted as a function of temperature. These data are tabulated together with the experimental conditions in Table S1. From Figure 2, it is apparent that there is a negative temperature dependence, no apparent dependence on pressure and that individual determinations of k_1 are highly reproducible. The high precision of the data allows a weak curvature to be observed, which was fitted using a modified Arrhenius expression, yielding the following expression for the temperature dependence of k_1:

$$k_1(T) = (3.7 \pm 1.4) \times 10^{-21} \times T^2 \times \exp((1710 \pm 103)/T) \quad (8)$$

The overall negative temperature dependence suggests that reaction 1 proceeds through a prereactive complex in the entrance channel.[44]

Reaction 2, $CH_2OO + C_2H_5OH$, was found to possess a similar rate coefficient to reaction 1. Figure 2 also shows k_2 versus temperature, with kinetic data and experimental conditions tabulated in Table S2. The precisions of the rate coefficient measurements approach those of reaction 1, allowing the observation of some curvature in the temperature dependence, which was fitted with the following modified Arrhenius expression:

$$k_2(T) = (4.2 \pm 2.2) \times 10^{-21} \times T^2 \times \exp((1717 \pm 145)/T) \quad (9)$$

Both the A-factor and the activation energy (E_a/R) are similar to those obtained for reaction 1, indicating that the carbon chain length on the alcohol does not have a strong influence over the reaction rate. Again, the formation of a prereactive complex in the initial reaction step is expected to be responsible for the negative temperature dependence observed.

3.2. Reaction of $(CH_3)_2COO$ with CH_3OH. Figure 3 shows a plot of k_3 versus temperature for reaction 3 $(CH_3)_2COO + CH_3OH$, with kinetic data and experimental conditions provided in Table S3. In contrast to reactions 1 and 2, reaction 3 shows an overall slower reaction rate with a strongly curved temperature dependence. In this instance, the curvature is such that the data are best described with a more complicated

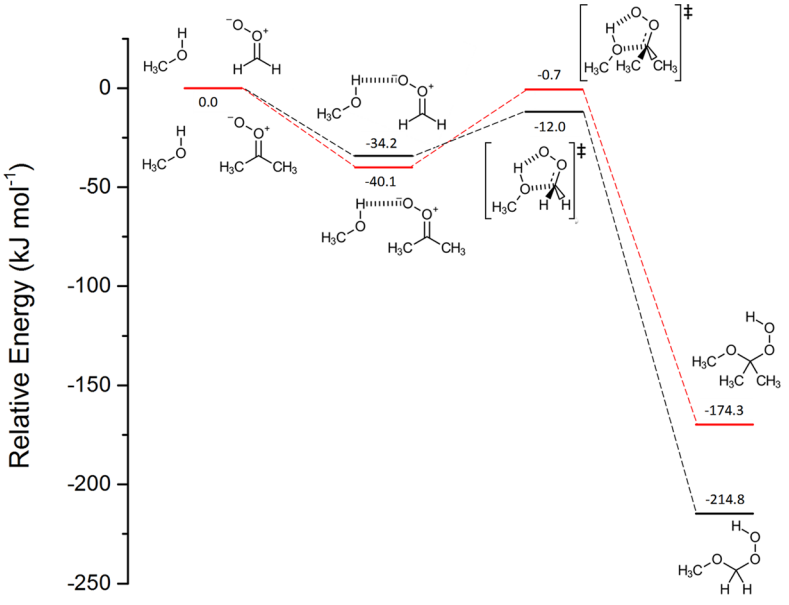

Figure 4. Potential energy calculations for the reactions of methanol with CH_2OO (black) and $(CH_3)_2COO$ (red). For CH_2OO, a lower barrier is observed, whereas for $(CH_3)_2COO$, the barrier that is encountered by reactants coming out of the prereactive complex energy well is significantly higher, which might explain the complicated temperature dependence observed for this reaction. Optimized structures for each of these species and complexes can be found in the Supporting Information.

DOI: 10.1021/acsearthspacechem.7b00108
ACS Earth Space Chem. 2017, 1, 664−672

function, and a sum of two expressions was used to describe both the positive and negative temperature-dependent components to the overall rate coefficient:

$$k_3(T) = 6.07 \times 10^{-33} \times T^{3.87} \times \exp(5852/T) + 5.82 \times 10^{-16} \times T^{2.92} \times \exp(-3741/T) \quad (10)$$

Because of the complexity of the above expression, these optimized values should not be considered to form a unique solution, and *A*-factors and activation energies should be treated with caution. However, taken at face value, the temperature dependencies therein are both highly positive and negative, respectively. One interpretation of the positive temperature-dependent component of this reaction is the agency of a hydrogen abstraction mechanism that operates parallel to the generally accepted insertion mechanism that forms AAAHs in these reactions.[18−20,45] To investigate this possibility further, rate coefficients were determined for a suite of deuterated isotopologues of methanol. As can be seen from Figure 3, no significant differences were observed between the isotopologues. This result indicates that hydrogen abstraction does not make a significant contribution to the overall rate coefficient under these conditions, and implies that the differences are likely to result solely from dissimilarities on the potential energy surfaces for the insertion reactions (see the following section for further discussion). In a prereactive complex-forming reaction such as this, there remains the potential for interfering absorption by the complex at the probe wavelength to affect the retrieved decay profiles. A kinetic analysis is presented in the Supporting Information, from which we conclude that such an outcome is unlikely.

4. DISCUSSION AND SUPPORTING CALCULATIONS

The similarity between $k(T)$ for reactions 1 and 2 indicates that the size of the alkyl chain of the alcohol has little effect on the rate coefficient for these reactions, and any differences appear to be limited to the *A*-factor. That deuteration of the alcohol moiety has no discernible effect on reaction 3 further implies that H/D transfer does not have a strong impact on the overall rate coefficient. In contrast, the substitution about the CI has a large influence over the reaction rate. One way of rationalizing this observation is that the barrier to forming the transition state that leads to products is higher in the case of reaction 3. This hypothesis is supported by potential energy calculations for reactions 1 and 3, shown in Figure 4, which suggest that both reactions 1 and 3 form prereactive complexes that are stabilized by a single hydrogen bond between the hydrogen of the alcohol moiety and the terminal oxygen of the CI moiety. The barrier to forming AAAH products is found to be submerged in both reactions 1 and 3; however, in the latter case, the transition state is very close to the energy of reactants. Furthermore, the prereactive complex is ∼6 kJ mol^{-1} lower in energy than in reaction 1, demonstrating that the local minimum in which the prereactive complex resides is significantly deeper in the case of reaction 3.

No absolute kinetic measurements are available in the literature with which reactions 1−3 can be compared, although the rate of reaction between methanol and the C_{13} CIs produced from 1-tetradecene ozonolysis has been determined relative to the reaction with heptanoic acid.[20] It is necessary to make several assumptions to put this relative rate onto the absolute scale (see section 6 for a full treatment) and, once performed, yields rate coefficients that are a factor of ∼2 larger than the absolute determinations of this work. Given that at least some of this difference may be physical between the C_{13} CIs and the smaller CIs of this work, and that no major cancellation of errors results from these assumptions, the level of agreement is satisfactory. This finding indicates that larger CIs, more representative of those formed in the atmosphere by ozonolysis and less likely to be consumed rapidly by water, behave in a similar way to the smaller CIs that are presented here. This comparison also shows that static chamber-based measurements can provide a suitable alternative to these absolute measurements, which become rapidly limited by vapor pressure as the size of the carbon backbone of the alkyl *gem*-diiodides increases.[46]

5. ATMOSPHERIC IMPLICATIONS

Based on the large flux of methanol to the atmosphere, it is clear that reactions 1 and 3 cannot represent an important tropospheric methanol sink. Accordingly, this discussion focuses on the products of these reactions, the AAAHs. A pair of main loss processes are considered here: the photolytic loss and the loss by reaction with OH radicals.

The UV absorption spectra of these peroxides have not been studied previously and to assess their photolysis lifetimes, a calculated spectrum for MMHP was obtained through the nuclear ensemble method described in the Methods section. Figure 5 compares this calculated spectrum with experimentally

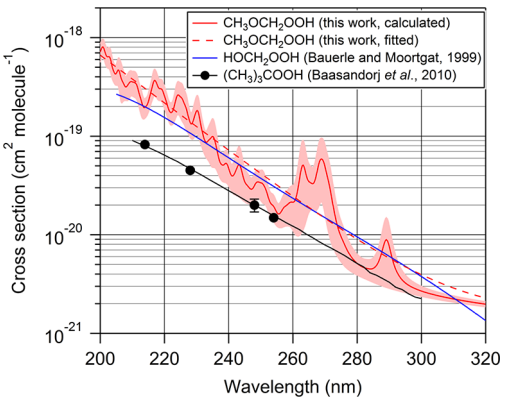

Figure 5. Calculated UV absorption cross-section for the simplest α-alkoxyalkyl hydroperoxide (AAAH), methoxymethyl hydroperoxide (MMHP). A close similarity is observed between MMHP and the literature measurement for hydroxymethyl hydroperoxide, suggesting a commonality in the photochemistry of AAAHs.

determined spectra for similar hydroperoxides available in the literature.[47,48] MMHP was found to possess four low-energy conformers, and the spectrum in Figure 5 represents an average that is weighted according to the abundance of each of these conformers (for the conformer-specific spectra and their free energies, see the Supporting Information). A striking similarity was observed between the computed absorption spectrum of MMHP and the most closely analogous compound, hydroxymethyl hydroperoxide, and as with this compound, the photolysis lifetime is therefore expected to be ∼4 days.[48]

This lifetime is long enough for oxidation by OH to become competitive. Although no rate coefficients of AAAHs + OH are available in the literature, measurements of other hydroperoxides indicate that the peroxidic hydrogen will be the dominant reactive site, with overall rate coefficients that range from ∼2−6 × 10^{-12} cm^3 molecule^{-1} s^{-1} at room temper-

DOI: 10.1021/acsearthspacechem.7b00108
ACS Earth Space Chem. 2017, 1, 664−672

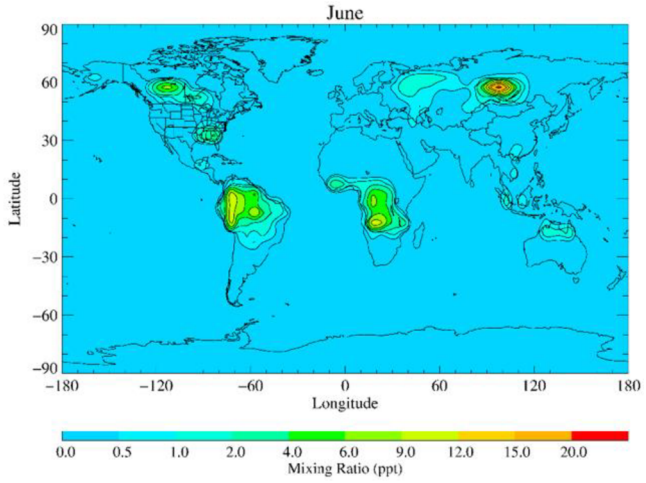

Figure 6. Global distribution of AAAHs formed in the atmosphere for the month of June. A strong co-location between AAAHs and the productive forested regions is observed, which is a consequence of the large terrestrial biospheric source of methanol and alkenes in these areas.

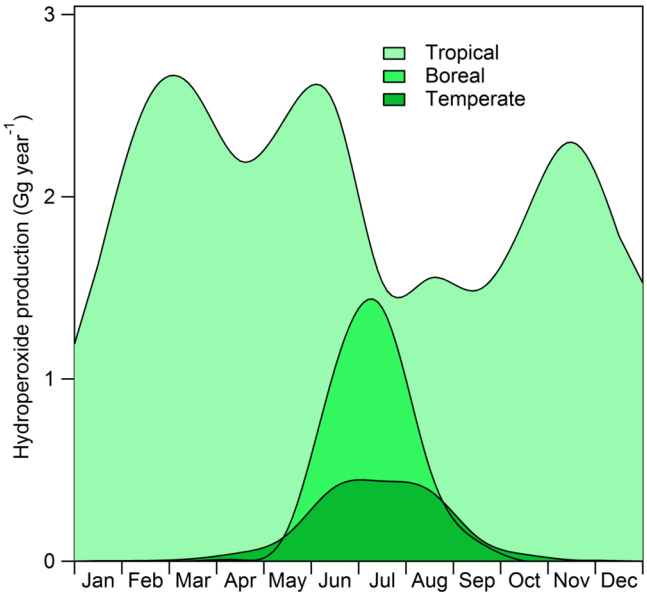

Figure 7. Production of AAAHs over the course of a year. Whereas tropical forests represent a dominant source throughout the year, boreal and temperate forests only contribute significantly during the northern hemispheric summer.

ature[47,49−52] and no clear dependence on alkyl substitution. With the additional ether functionality of AAAHs, it is expected that these hydroperoxides will tend toward the more reactive end, and if 6×10^{-12} cm^3 molecule^{-1} s^{-1} is representative of the AAAHs, this leads to a lifetime of ∼2 days, assuming an average OH concentration of 1×10^6 molecule cm^{-3}. Reaction with OH will therefore be the main removal process, but photolysis will also be significant.

These atmospheric sinks of AAAHs were incorporated into a global chemistry transport modeling simulation, together with the source terms described in section 2.4 (details on the rate coefficients employed can be found in Table S4). Global mixing ratios of AAAHs are provided in Figure 6 for the month of June, when the biogenic emissions of methanol and CI precursors from the boreal forests are at a maximum. Figure 7 shows monthly production rates, indicating that the tropical forests represent a dominant source throughout the year (24 Gg year^{-1}), with a minimum between July and September, during the dry season in the southern tropics. In contrast, the boreal forests produce a maximum between June and August, falling off rapidly on either side, with an annual flux of 3 Gg year^{-1}. Temperate forests are the smallest source of AAAHs considered, with a production rate of 2 Gg year^{-1}, showing a similar seasonality to the boreal forests.

Although the present calculations suggest that AAAHs will constitute a radical source in the troposphere, the formation of larger, more-functionalized AAAHs derived from the reactions of more-complicated CIs, alcohols, or the secondary oxidation of primary AAAHs may have a subtler role to play in the formation of SOA.

6. COMPARISON WITH LITERATURE MEASUREMENTS

Tobias and Ziemann[20] reported a room-temperature relative rate for the reaction of a C_{13} Criegee intermediate produced from 1-tetradecene ozonolysis:

$$1 - C_{14}H_{28} + O_3 \rightarrow \textit{syn}\text{-} / \textit{anti}\text{-}C_{13}H_{26}OO + CH_2O \quad (11a)$$

$$\rightarrow CH_2OO + C_{13}H_{26}O \quad (11b)$$

where heptanoic acid was employed as a reference reagent. Given that reaction 11 produces both *syn* and *anti* conformers, this relative rate is interpreted as follows:

$$\frac{(k_{syn-C_{13}H_{26}OO+CH_3OH} \cdot x_{syn}) + (k_{anti-C_{13}H_{26}OO+CH_3OH} \cdot (1 - x_{syn}))}{k_{syn\text{-}/anti\text{-}C_{13}H_{26}OO+\text{heptanoic acid}}} = 0.0013 \quad (12)$$

Comparison of the current results necessitates several assumptions. First, $k_{syn\text{-}/anti\text{-}C_{13}H_{26}OO + \text{heptanoic acid}}$ is taken to be a generic rate coefficient of 1×10^{-10} cm^3 molecule^{-1} s^{-1} for all organic acid + CI reactions, with no conformer dependence ascribed.[9] Second, in the absence of experimental data, an assumption must be made regarding the molar branching ratio for formation of the *syn* and *anti* CIs, x_{syn} and $1 - x_{syn}$ in eq 12. One way to approach this is to take the OH yield from analogous terminal alkenes.

Scheme 1 shows how OH radicals are produced from long-chain terminal alkene ozonolysis. Terminal alkenes such as 1-hexene, 1-heptene and 1-octene have overall OH yields from ozonolysis of ∼0.33.[53,54] These compounds are known to

Scheme 1. OH Radical Production from Long-Chain Terminal Alkene Ozonolysis

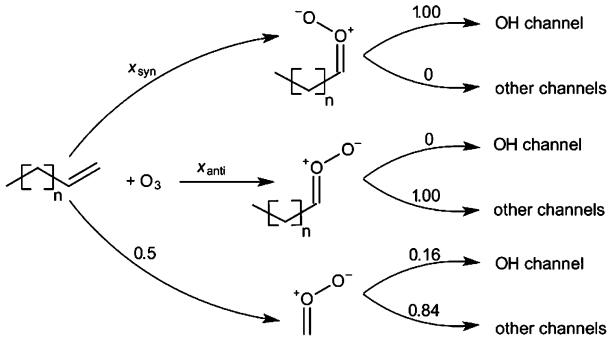

DOI: 10.1021/acsearthspacechem.7b00108
ACS Earth Space Chem. 2017, 1, 664−672

produce CH_2OO in a molar yield (x_{CH_2OO}) of ~0.5.[53] The OH yield of CH_2OO produced through ozonolysis has been determined to be 0.16.[53] Rickard et al.[54] recommend that *syn*-CIs have a unit OH yield, whereas *anti*-CIs do not yield OH, and the overall OH yield can therefore be described as follows:

$$1.0 \times x_{syn} + (0.16 \times x_{CH_2OO}) = 0.33 \quad (13)$$

which gives a value for x_{syn} of 0.25. Because the three possible CIs formed must sum to a yield of one, the yield of *anti*-CI (x_{anti}) will be 0.25 as well.

The third assumption is that the ratio of rate coefficients for *syn*- and *anti*-$C_{13}H_{26}OO$ is similar to that of k_3 and k_1 measured in this study (0.42 at 298 K); in the case of $(CH_3)_2COO$, the terminal oxygen atom always faces toward an alkyl substitution and is considered to be representative of a purely *syn*-CI, whereas CH_2OO never faces an alkyl substitution and is considered to be purely *anti* in character. Because the relative rate coefficient of Tobias and Ziemann[20] only considers the fate of the $C_{13}H_{26}OO$ CIs, the above values of 0.25 are effectively doubled, and by accounting for the ratio of k_1 and k_3 from this study, eq 12 is simplified as follows:

$$\frac{k_{anti} \times 0.71}{1 \times 10^{-10}} = 0.0013 \quad (14)$$

from which individual rate coefficient values of 2×10^{-13} and 8×10^{-14} cm^3 molecule^{-1} s^{-1} can be obtained for *anti*- and *syn*-$C_{13}H_{26}OO$, respectively. These values are a factor of 2 larger than the rate coefficients determined in this work. This comparison suggests that the static chamber ozonolysis experiments, if conducted under the right conditions, are a reliable source of kinetic data for the reactions of large CIs that cannot be accessed through the direct methodology employed in this work.

7. CONCLUSIONS

Direct experimental rate coefficient measurements for the reactions of CH_2OO and $(CH_3)_2COO$ + methanol and that of CH_2OO + ethanol are presented. Experimental conditions were varied between temperatures of 254 and 329 K and pressures of 10 and 100 Torr (N_2), with no evidence of pressure dependence, and a strong non-Arrhenius temperature dependence was observed in all cases. The rate coefficient of $(CH_3)_2COO$ + methanol exhibited both a negative and positive temperature-dependent component, which may in part be explained by a higher barrier encountered by the prereactive complex as it proceeds to product formation. It is acknowledged, however, that this alone is insufficient to explain the extent of the temperature dependence observed, and a more rigorous theoretical treatment is required. The insertion reactions by which CIs react with alcohols produce α-alkoxyalkyl hydroperoxides (AAAHs). The calculated UV cross-section of a representative of these species, methoxymethyl hydroperoxide (MMHP), is found to be similar to other peroxides, indicating that, while tropospheric photolysis is an important sink for these species, oxidation and deposition are likely to be competitive. Based on these findings, a global chemistry transport model is used to estimate the abundance and flux of AAAHs into the global atmosphere. A total flux of ~30 Gg year^{-1} is obtained, with most production occurring in the tropical forests, where biogenic methanol and alkene emissions are both high.

■ ASSOCIATED CONTENT

Supporting Information

The Supporting Information is available free of charge on the ACS Publications website at DOI: 10.1021/acsearthspacechem.7b00108.

Tabulated experimental data and conditions. Computational details for UV cross-section and potential energy calculations, kinetic parameters employed in atmospheric chemical modeling, NMR spectra for the $(CH_3)_2CI_2$ sample, and a kinetic analysis of experimental observations. (PDF)

■ AUTHOR INFORMATION

Corresponding Authors

*E-mail: max.mcgillen@gmail.com.
*E-mail: a.orr-ewing@bristol.ac.uk.

ORCID

Max R. McGillen: 0000-0002-1623-5985
M. Anwar H. Khan: 0000-0001-7836-3344
Andrew J. Orr-Ewing: 0000-0001-5551-9609

Notes

The authors declare no competing financial interest.
All experimental data are archived in the University of Bristol's Research Data Storage Facility (https://data.bris.ac.uk/data/dataset/15u01cg9sxkkx2vma4nwh6nxf3).

■ ACKNOWLEDGMENTS

Funding for this work by NERC grant nos. NE/K004905/1 and NE/P013104/1 is gratefully acknowledged. M.R.M., J.M.B., and B.F.E.C. are supported by Marie Skłodowska-Curie Individual Fellowships HOMER (702794), NPTC (701593), and NAMDIA (710355), respectively. We thank Prof. G.C. Lloyd-Jones and Drs C. Nottingham and T. West (University of Edinburgh) for the 2,2-diiodopropane sample.

■ REFERENCES

(1) Johnson, D.; Marston, G. The Gas-phase Ozonolysis of Unsaturated Volatile Organic Compounds in the Troposphere. *Chem. Soc. Rev.* **2008**, *37* (4), 699−716.

(2) Anglada, J. M.; Gonzalez, J.; Torrent-Sucarrat, M. Effects of the Substituents on the Reactivity of Carbonyl Oxides. A Theoretical Study on the Reaction of Substituted Carbonyl Oxides with Water. *Phys. Chem. Chem. Phys.* **2011**, *13* (28), 13034−13045.

(3) Smith, M. C.; Chang, C. H.; Chao, W.; Lin, L. C.; Takahashi, K.; Boering, K. A.; Lin, J. J. M. Strong Negative Temperature Dependence of the Simplest Criegee Intermediate CH_2OO Reaction with Water Dimer. *J. Phys. Chem. Lett.* **2015**, *6* (14), 2708−2713.

(4) Huang, H. L.; Chao, W.; Lin, J. J. M. Kinetics of a Criegee Intermediate that would Survive High Humidity and may Oxidize Atmospheric SO_2. *Proc. Natl. Acad. Sci. U. S. A.* **2015**, *112* (35), 10857−10862.

(5) Chhantyal-Pun, R.; Davey, A.; Shallcross, D. E.; Percival, C. J.; Orr-Ewing, A. J. A Kinetic Study of the CH_2OO Criegee Intermediate Self-reaction, Reaction with SO_2 and Unimolecular Reaction using Cavity Ring-down Spectroscopy. *Phys. Chem. Chem. Phys.* **2015**, *17* (5), 3617−3626.

(6) Novelli, A.; Hens, K.; Ernest, C. T.; Martinez, M.; Nölscher, A. C.; Sinha, V.; Paasonen, P.; Petäjä, T.; Sipilä, M.; Elste, T.; Plass-Dülmer, C.; Phillips, G. J.; Kubistin, D.; Williams, J.; Vereecken, L.; Lelieveld, J.; Harder, H. Estimating the atmospheric concentration of Criegee intermediates and their possible interference in a FAGE-LIF instrument. *Atmos. Chem. Phys.* **2017**, *17*, 7807−7826.

(7) Berndt, T.; Jokinen, T.; Sipila, M.; Mauldin, R. L.; Herrmann, H.; Stratmann, F.; Junninen, H.; Kulmala, M. H_2SO_4 Formation from the

DOI: 10.1021/acsearthspacechem.7b00108
ACS Earth Space Chem. 2017, 1, 664−672

Gas-phase Reaction of Stabilized Criegee Intermediates with SO_2: Influence of Water Vapour Content and Temperature. *Atmos. Environ.* **2014**, *89*, 603−612.
(8) Mauldin, R. L., III; Berndt, T.; Sipila, M.; Paasonen, P.; Petaja, T.; Kim, S.; Kurten, T.; Stratmann, F.; Kerminen, V. M.; Kulmala, M. A new atmospherically relevant oxidant of sulphur dioxide. *Nature* **2012**, *488* (7410), 193−196.
(9) Welz, O.; Eskola, A. J.; Sheps, L.; Rotavera, B.; Savee, J. D.; Scheer, A. M.; Osborn, D. L.; Lowe, D.; Booth, A. M.; Xiao, P.; Khan, M. A. H.; Percival, C. J.; Shallcross, D. E.; Taatjes, C. A. Rate Coefficients of C1 and C2 Criegee Intermediate Reactions with Formic and Acetic Acid Near the Collision Limit: Direct Kinetics Measurements and Atmospheric Implications. *Angew. Chem., Int. Ed.* **2014**, *53* (18), 4547−4550.
(10) Chhantyal-Pun, R.; McGillen, M. R.; Beames, J. M.; Khan, M. A. H.; Percival, C. J.; Shallcross, D. E.; Orr-Ewing, A. J. Temperature Dependence of the Rates of Reaction of Trifluoroacetic Acid with Criegee Intermediates. *Angew. Chem., Int. Ed.* **2017**, *56* (31), 9044−9047.
(11) Buras, Z. J.; Elsamra, R. M. I.; Jalan, A.; Middaugh, J. E.; Green, W. H. Direct Kinetic Measurements of Reactions between the Simplest Criegee Intermediate CH_2OO and Alkenes. *J. Phys. Chem. A* **2014**, *118* (11), 1997−2006.
(12) Elsamra, R. M. I.; Jalan, A.; Buras, Z. J.; Middaugh, J. E.; Green, W. H. Temperature- and Pressure-dependent Kinetics of CH_2OO + CH_3COCH_3 and CH_2OO + CH_3CHO: Direct Measurements and Theoretical Analysis. *Int. J. Chem. Kinet.* **2016**, *48* (8), 474−488.
(13) Sakamoto, Y.; Yajima, R.; Inomata, S.; Hirokawa, J. Water Vapour Effects on Secondary Organic Aerosol Formation in Isoprene Ozonolysis. *Phys. Chem. Chem. Phys.* **2017**, *19* (4), 3165−3175.
(14) Vereecken, L.; Rickard, A. R.; Newland, M. J.; Bloss, W. J. Theoretical Study of the Reactions of Criegee Intermediates with Ozone, Alkylhydroperoxides, and Carbon Monoxide. *Phys. Chem. Chem. Phys.* **2015**, *17* (37), 23847−23858.
(15) Goldan, P. D.; Kuster, W. C.; Fehsenfeld, F. C.; Montzka, S. A. The Observation of a C5 Alcohol Emission in a North-American Pine Forest. *Geophys. Res. Lett.* **1993**, *20* (11), 1039−1042.
(16) Stavrakou, T.; Guenther, A.; Razavi, A.; Clarisse, L.; Clerbaux, C.; Coheur, P. F.; Hurtmans, D.; Karagulian, F.; De Maziere, M.; Vigouroux, C.; Amelynck, C.; Schoon, N.; Laffineur, Q.; Heinesch, B.; Aubinet, M.; Rinsland, C.; Muller, J. F. First Space-based Derivation of the Global Atmospheric Methanol Emission Fluxes. *Atmos. Chem. Phys.* **2011**, *11* (10), 4873−4898.
(17) Leather, K. E.; McGillen, M. R.; Cooke, M. C.; Utembe, S. R.; Archibald, A. T.; Jenkin, M. E.; Derwent, R. G.; Shallcross, D. E.; Percival, C. J. Acid-yield Measurements of the Gas-phase Ozonolysis of Ethene as a Function of Humidity using Chemical Ionisation Mass Spectrometry (CIMS). *Atmos. Chem. Phys.* **2012**, *12* (1), 469−479.
(18) Dussault, P.; Sahli, A. 2-Methoxyprop-2-yl Hydroperoxide - a Convenient Reagent for the Synthesis of Hydroperoxides and Peracids. *J. Org. Chem.* **1992**, *57* (3), 1009−1012.
(19) Neeb, P.; Horie, O.; Moortgat, G. K. Gas-phase Ozonolysis of Ethene in the Presence of Hydroxylic Compounds. *Int. J. Chem. Kinet.* **1996**, *28* (10), 721−730.
(20) Tobias, H. J.; Ziemann, P. J. Kinetics of the Gas-phase Reactions of Alcohols, Aldehydes, Carboxylic Acids, and Water with the C13 Stabilized Criegee Intermediate Formed from Ozonolysis of 1-Tetradecene. *J. Phys. Chem. A* **2001**, *105* (25), 6129−6135.
(21) Welz, O.; Savee, J. D.; Osborn, D. L.; Vasu, S. S.; Percival, C. J.; Shallcross, D. E.; Taatjes, C. A. Direct Kinetic Measurements of Criegee Intermediate (CH_2OO) Formed by Reaction of CH_2I with O_2. *Science* **2012**, *335* (6065), 204−207.
(22) Frisch, M. J.; Trucks, G. W.; Schlegel, H. B.; Scuseria, G. E.; Robb, M. A.; Cheeseman, J. R.; Scalmani, G.; Barone, V.; Petersson, G. A.; Nakatsuji, H.; Li, X.; Caricato, M.; Marenich, A.; Bloino, J.; Janesko, B. G.; Gomperts, R.; Mennucci, B.; Hratchian, H. P.; Ortiz, J. V.; Izmaylov, A. F.; Sonnenberg, J. L.; Williams-Young, D.; Ding, F.; Lipparini, F.; Egidi, F.; Goings, J.; Peng, B.; Petrone, A.; Henderson, T.; Ranasinghe, D.; Zakrzewski, V. G.; Gao, J.; Rega, N.; Zheng, G.; Liang, W.; Hada, M.; Ehara, M.; Toyota, K.; Fukuda, R.; Hasegawa, J.; Ishida, M.; Nakajima, T.; Honda, Y.; Kitao, O.; Nakai, H.; Vreven, T.; Throssell, K.; Montgomery, J. A.; Peralta, J. J. E.; Ogliaro, F.; Bearpark, M.; Heyd, J. J.; Brothers, E.; Kudin, K. N.; Staroverov, V. N.; Keith, T.; Kobayashi, R.; Normand, J.; Raghavachari, K.; Rendell, A.; Burant, J. C.; Iyengar, S. S.; Tomasi, J.; Cossi, M.; Millam, J. M.; Klene, M.; Adamo, C.; Cammi, R.; Ochterski, J. W.; Martin, R. L.; Morokuma, K.; Farkas, O.; Foresman, J. B.; Fox, D. J. *Gaussian 09, Revision D.01*; Gaussian, Inc.: Wallingford, CT, 2016.
(23) Werner, H. J.; Knowles, P. J.; Knizia, G.; Manby, F. R.; Schütz, M.; Celani, P.; Györffy, W.; Kats, D.; Korona, T.; Lindh, R.; Mitrushenkov, A.; Rauhut, G.; Shamasundar, K. R.; Adler, T. B.; Amos, R. D.; Bernhardsson, A.; Berning, A.; Cooper, D. L.; Deegan, M. J. O.; Dobbyn, A. J.; Eckert, F.; Goll, E.; Hampel, C.; Hesselmann, A.; Hetzer, G.; Hrenar, T.; Jansen, G.; Köppl, C.; Liu, Y.; Lloyd, A. W.; Mata, R. A.; May, A. J.; McNicholas, S. J.; Meyer, W.; Mura, M. E.; Nicklaß, A.; O'Neill, D. P.; Palmieri, P.; Peng, D.; Pflüger, K.; Pitzer, R.; Reiher, M.; Shiozaki, T.; Stoll, H.; Stone, A. J.; Tarroni, R.; Thorsteinsson, T.; Wang, M. *MOLPRO*; TGZ Molpro: Stuttgart, Germany, 2017.
(24) Miliordos, E.; Xantheas, S. S. The Origin of the Reactivity of the Criegee Intermediate: Implications for Atmospheric Particle Growth. *Angew. Chem., Int. Ed.* **2016**, *55* (3), 1015−1019.
(25) Frisch, M. J.; Head-Gordon, M.; Pople, J. A. A Direct MP2 Gradient-Method. *Chem. Phys. Lett.* **1990**, *166* (3), 275−280.
(26) Head-Gordon, M.; Head-Gordon, T. Analytic MP2 Frequencies without 5th-Order Storage - Theory and Application to Bifurcated Hydrogen-Bonds in the Water Hexamer. *Chem. Phys. Lett.* **1994**, *220* (1−2), 122−128.
(27) Head-Gordon, M.; Pople, J. A.; Frisch, M. J. MP2 Energy Evaluation by Direct Methods. *Chem. Phys. Lett.* **1988**, *153* (6), 503−506.
(28) Møller, C.; Plesset, M. S. Note on an Approximation Treatment for Many-electron Systems. *Phys. Rev.* **1934**, *46* (7), 618−622.
(29) Dunning, T. H. Gaussian-Basis Sets for Use in Correlated Molecular Calculations 0.1. The Atoms Boron through Neon and Hydrogen. *J. Chem. Phys.* **1989**, *90* (2), 1007−1023.
(30) Barbatti, M.; Aquino, A. J. A.; Lischka, H. The UV Absorption of Nucleobases: Semi-classical Ab Initio Spectra Simulations. *Phys. Chem. Chem. Phys.* **2010**, *12* (19), 4959−4967.
(31) Barbatti, M.; Sen, K. Effects of Different Initial Condition Samplings on Photodynamics and Spectrum of Pyrrole. *Int. J. Quantum Chem.* **2016**, *116* (10), 762−771.
(32) Crespo-Otero, R.; Barbatti, M. Spectrum Simulation and Decomposition with Nuclear Ensemble: Formal Derivation and Application to Benzene, Furan and 2-Phenylfuran. *Theor. Chem. Acc.* **2012**, *131* (6), 1237.
(33) Barbatti, M.; Granucci, G.; Ruckenbauer, M.; Plasser, F.; Crespo-Otero, R.; Pittner, J.; Persico, M.; Lischka, H. *NEWTON-X: A Package for Newtonian Dynamics Close to the Crossing Seam*, Version 1.4; NEWTON-X: Mülheim an der Ruhr, Germany, 2017; www.newtonx.org.
(34) Barbatti, M.; Ruckenbauer, M.; Plasser, F.; Pittner, J.; Granucci, G.; Persico, M.; Lischka, H. Newton-X: A Surface-hopping Program for Nonadiabatic Molecular Dynamics. *Wires Comput. Mol. Sci.* **2014**, *4* (1), 26−33.
(35) Christiansen, O.; Koch, H.; Jorgensen, P. The 2nd-Order Approximate Coupled-Cluster Singles and Doubles Model CC2. *Chem. Phys. Lett.* **1995**, *243* (5−6), 409−418.
(36) Grimme, S. Improved Second-order Møller-Plesset Perturbation Theory by Separate Scaling of Parallel- and Antiparallel-spin Pair Correlation Energies. *J. Chem. Phys.* **2003**, *118* (20), 9095−9102.
(37) Hellweg, A.; Grün, S. A.; Hättig, C. Benchmarking the Performance of Spin-component Scaled CC2 in Ground and Electronically Excited States. *Phys. Chem. Chem. Phys.* **2008**, *10* (28), 4119−4127.
(38) Furche, F.; Ahlrichs, R.; Hättig, C.; Klopper, W.; Sierka, M.; Weigend, F. Turbomole. *Wires Comput. Mol. Sci.* **2014**, *4* (2), 91−100.

DOI: 10.1021/acsearthspacechem.7b00108
ACS Earth Space Chem. 2017, 1, 664−672

(39) Korona, T.; Werner, H. J. Local Treatment of Electron Excitations in the EOM-CCSD Method. *J. Chem. Phys.* **2003**, *118* (7), 3006−3019.
(40) Utembe, S. R.; Cooke, M. C.; Archibald, A. T.; Jenkin, M. E.; Derwent, R. G.; Shallcross, D. E. Using a Reduced Common Representative Intermediates (CRIv2-R5) Mechanism to Simulate Tropospheric Ozone in a 3-D Lagrangian Chemistry Transport Model. *Atmos. Environ.* **2010**, *44* (13), 1609−1622.
(41) Guenther, A. B.; Jiang, X.; Heald, C. L.; Sakulyanontvittaya, T.; Duhl, T.; Emmons, L. K.; Wang, X. The Model of Emissions of Gases and Aerosols from Nature version 2.1 (MEGAN2.1): An Extended and Updated Framework for Modeling Biogenic Emissions. *Geosci. Model Dev.* **2012**, *5* (6), 1471−1492.
(42) Percival, C. J.; Welz, O.; Eskola, A. J.; Savee, J. D.; Osborn, D. L.; Topping, D. O.; Lowe, D.; Utembe, S. R.; Bacak, A.; McFiggans, G.; Cooke, M. C.; Xiao, P.; Archibald, A. T.; Jenkin, M. E.; Derwent, R. G.; Riipinen, I.; Mok, D. W. K.; Lee, E. P. F.; Dyke, J. M.; Taatjes, C. A.; Shallcross, D. E. Regional and Global Impacts of Criegee Intermediates on Atmospheric Sulphuric Acid Concentrations and First Steps of Aerosol Formation. *Faraday Discuss.* **2013**, *165*, 45−73.
(43) Chhantyal-Pun, R.; Welz, O.; Savee, J. D.; Eskola, A. J.; Lee, E. P. F.; Blacker, L.; Hill, H. R.; Ashcroft, M.; Khan, M. A. H.; Lloyd-Jones, G. C.; Evans, L.; Rotavera, B.; Huang, H. F.; Osborn, D. L.; Mok, D. K. W.; Dyke, J. M.; Shallcross, D. E.; Percival, C. J.; Orr-Ewing, A. J.; Taatjes, C. A. Direct Measurements of Unimolecular and Bimolecular Reaction Kinetics of the Criegee Intermediate $(CH_3)_2COO$. *J. Phys. Chem. A* **2017**, *121* (1), 4−15.
(44) Donahue, N. M. Reaction Barriers: Origin and Evolution. *Chem. Rev.* **2003**, *103* (12), 4593−4604.
(45) Criegee, R. Mechanism of Ozonolysis. *Angew. Chem., Int. Ed. Engl.* **1975**, *14* (11), 745−752.
(46) Yaws, C. L. *The Yaws Handbook of Vapor Pressure: Antoine Coefficients*, 2 ed.; Elsevier: Oxford, England, 2015.
(47) Baasandorj, M.; Papanastasiou, D. K.; Talukdar, R. K.; Hasson, A. S.; Burkholder, J. B. $(CH_3)_3COOH$ (Tert-butyl Hydroperoxide): OH Reaction Rate Coefficients Between 206 and 375 K and the OH Photolysis Quantum Yield at 248 nm. *Phys. Chem. Chem. Phys.* **2010**, *12* (38), 12101−12111.
(48) Bauerle, S.; Moortgat, G. K. Absorption Cross-sections of $HOCH_2OOH$ Vapor Between 205 and 360 nm at 298 K. *Chem. Phys. Lett.* **1999**, *309* (1−2), 43−48.
(49) Anastasi, C.; Smith, I. W. M.; Parkes, D. A. Flash-photolysis Study of Spectra of CH_3O_2 and $C(CH_3)_3O_2$ Radicals and Kinetics of their Mutual Reactions and with NO. *J. Chem. Soc., Faraday Trans. 1* **1978**, *74*, 1693−1701.
(50) Atkinson, R.; Baulch, D. L.; Cox, R. A.; Crowley, J. N.; Hampson, R. F.; Hynes, R. G.; Jenkin, M. E.; Rossi, M. J.; Troe, J. IUPAC Task Group on Atmospheric Chemical Kinetic Data Evaluation. http://iupac.pole-ether.fr, accessed November 2017.
(51) Blitz, M. A.; Heard, D. E.; Pilling, M. J. Wavelength Dependent Photodissociation of CH_3OOH - Quantum Fields for CH_3O and OH, and Measurement of the $OH+CH_3OOH$ Rate Coefficient. *J. Photochem. Photobiol., A* **2005**, *176* (1−3), 107−113.
(52) Vaghjiani, G. L.; Ravishankara, A. R. Kinetics and Mechanism of OH Reaction with CH_3OOH. *J. Phys. Chem.* **1989**, *93* (5), 1948−1959.
(53) Atkinson, R. Gas-phase Tropospheric Chemistry of Volatile Organic Compounds 1. Alkanes and Alkenes. *J. Phys. Chem. Ref. Data* **1997**, *26* (2), 215−290.
(54) Rickard, A. R.; Johnson, D.; McGill, C. D.; Marston, G. OH Yields in the Gas-phase Reactions of Ozone with Alkenes. *J. Phys. Chem. A* **1999**, *103* (38), 7656−7664.

DOI: 10.1021/acsearthspacechem.7b00108
ACS Earth Space Chem. 2017, 1, 664−672